Int J Thermophys (2010) 31:949–965
DOI 10.1007/s10765-010-0704-1

Thermophysical Properties of Liquid AlTi-Based Alloys

I. Egry · D. Holland-Moritz · R. Novakovic · E. Ricci · R. Wunderlich · N. Sobczak

Received: 19 June 2009 / Accepted: 15 January 2010 / Published online: 6 February 2010

Abstract The surface tension and density of three liquid AlTi-based alloys (AlTiV, AlTiNb, and AlTiTa) have been measured using electromagnetic levitation as a tool for containerless processing. Surface tension has been determined by the oscillating-drop method, while the density was measured using a shadowgraph technique. Both quantities were determined over a wide temperature range, including the undercooled regime. In addition, sessile-drop and pendant-drop experiments to determine the surface tension were performed in a recently built high-temperature furnace. The measured data were compared to thermodynamic calculations using phenomenological models and the Butler equation. Generally, good agreement was found.

Keywords Levitated drop · Liquid metals · Pendant drop · Sessile drop · Surface tension · Thermodynamic modeling · Titanium aluminides

1 Introduction

Titanium-based alloys have always been the focus for applications due to their light weight, high-temperature resistance, and biocompatibility. An entire conference series,

I. Egry (✉) · D. Holland-Moritz
Institut für Materialphysik im Weltraum, German Aerospace Center DLR, Cologne, Germany
e-mail: ivan.egry@dlr.de

R. Novakovic · E. Ricci
Institute for Energetics and Interphases, National Research Council CNR, Genoa, Italy

R. Wunderlich
Institute for Micro and Nanomaterials, University of Ulm, Ulm, Germany

N. Sobczak
Foundry Research Institute (CHTS), Cracow, Poland

the World Titanium Conference [1], is exclusively devoted to the science and technology of these alloys. Among them, $Ti_{90}Al_6V_4$ (Ti64) is widely used, in particular, for biomedical applications [2], whereas intermetallic titanium aluminides have received much interest as materials for turbine blades. Among them, $Al_{46}Ti_{46}Nb_8$ and $Al_{46}Ti_{46}Ta_8$ have been considered as castable alloys in the IMPRESS project [3].[1]

Industrial metallurgical processes, such as casting, are nowadays simulated numerically before real casting trials are made. These simulations require, as key parameters, thermophysical properties of the liquid alloy, in particular, the density, surface tension, and viscosity. Whereas the measurement of the viscosity faces unsurmountable experimental difficulties, we were able to measure the surface tension and density of the above mentioned AlTi-based alloys, using electromagnetic levitation (EML) as a containerless technique on the one hand, and the pendant-drop (PD) technique in a newly built high-temperature furnace on the other hand. The data obtained show excellent agreement and are presented below.

The experimental data are complemented by thermodynamic modeling of the binary AlTi alloy using different expressions for the thermodynamic potentials, and different models to relate the thermophysical properties to thermodynamics. In particular, the predictions by the models describing the surface tension compare favorably with the experimental data.

2 Measurements

For all measurements, samples from the same batch have been used. The $Ti_{90}Al_6V_4$ samples were made from commercially pure material, supplied by Johnson-Matthey, whereas the $Al_{46}Ti_{46}Nb_8$ and $Al_{46}Ti_{46}Ta_8$ alloys were supplied by the IMPRESS project. The oxygen content was not determined.

2.1 Density

The density of stable and deeply undercooled melts has been investigated by the levitated drop method. The experiments have been carried out under an inert Ar atmosphere of 6N purity. The oxygen partial pressure was not determined in situ. The temperature of the samples is contactlessly measured with a one color pyrometer. In order to determine the density of the melt, the samples were illuminated by a He–Ne laser beam and the shadowgraph of the sample was recorded by use of a CCD camera. Under the assumption that the shape of the specimen is axially symmetric, the density of the melt is inferred from the edge profile of the shadowgraph. The experimental setup and the data evaluation procedure are described in detail in [4]. The results of the investigations obtained for $Al_{46}Ti_{46}Nb_8$, $Al_{46}Ti_{46}Ta_8$, and Ti_{64} samples are shown in Fig. 1, together with earlier data on the $Ti_{47}Al_{44}Nb_8B_1$ alloy [5]. For the alloy containing Nb, a broad temperature range is covered, ranging from 1,580 K up to 1,960 K ($T_L = 1,843$ K), while the $Al_{46}Ti_{46}Ta_8$ alloy was more difficult to process due to

[1] Please note that for Ti64 the composition is given in mass%, whereas the composition of the other two alloys is in at%.

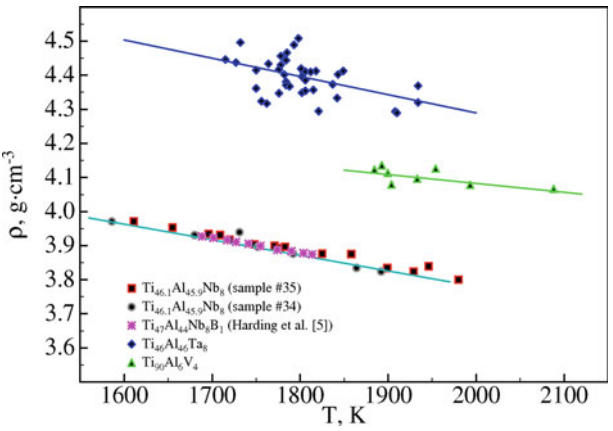

Fig. 1 Density of liquid $Al_{46}Ti_{46}Nb_8$, $Al_{46}Ti_{46}Ta_8$, and $Al_6Ti_{90}V_4$ as a function of temperature

Table 1 Density of AlTi-based alloys

Alloy	T_L (K)	$\rho_L(g \cdot cm^{-3})$	$-\rho_T(10^{-4} g \cdot cm^{-3} \cdot K^{-1})$
$Al_{46}Ti_{46}Nb_8$	1,843	3.85	4.6
$Al_{46}Ti_{46}Ta_8$	1,890	4.34	5.4
$Al_6Ti_{90}V_4$	1,933	4.1	2.6

its higher density. This is also the reason for the relatively large scatter in these data. Nevertheless, a temperature range of $\Delta T = 250\,K$ could be covered, including the undercooled regime ($T_L = 1{,}894\,K$), and an uncertainty of approximately 2 % could be maintained.

In the temperature range considered, the temperature dependence of the density of all alloys can be described by the following linear fit:

$$\rho = \rho_L + \rho_T(T - T_L). \tag{1}$$

Numerical values for T_L, ρ_L, and ρ_T are given in Table 1.

2.2 Surface Tension

2.2.1 Electromagnetic Levitation

The surface tension of stable and undercooled AlTi-based melts is measured by use of the same EML device that was also utilized for the density measurements described above. For determination of the surface tension, the oscillating-droplet method [6] is applied. The oscillations of the sample surface are recorded from the top of the levitator with a video camera at a frame rate of 400 Hz with a pixel resolution of $1{,}024 \times 1{,}000$ pixels. At each investigated temperature, a series of 4,096 frames is acquired.

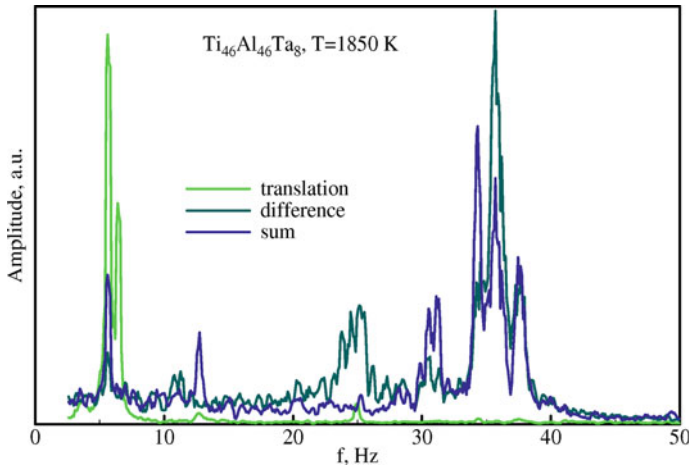

Fig. 2 Oscillation spectrum of a liquid levitated $Al_{46}Ti_{46}Ta_8$ drop

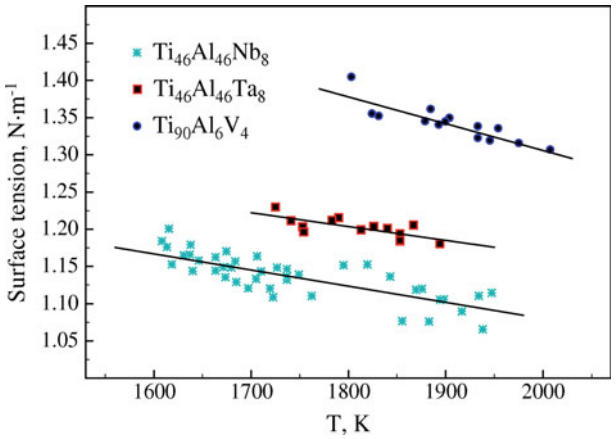

Fig. 3 Surface tensions of liquid $Al_{46}Ti_{46}Nb_8$, $Al_{46}Ti_{46}Ta_8$, and $Al_6Ti_{90}V_4$ as functions of temperature

From the video sequences, frequency spectra of the sample radius, R, are determined. Under microgravity, the spectrum consists of a single peak, corresponding to the Rayleigh frequency ω_R. It is related to the surface tension, σ, by

$$\sigma = \frac{3M}{32\pi}\omega_R^2. \tag{2}$$

Here, M denotes the sample mass. Measurements of the surface tension of the Al–Ti–X alloys have been performed during several parabolic flights, offering about 20 s of microgravity. Results are reported in Table 2.

Under terrestrial conditions, the oscillation spectrum contains five peaks at frequencies ω_i ($i = -2, -1, 0, 1, 2$) resulting from symmetry breaking by the gravitational

and levitation field. Moreover, three translational frequencies T_x, T_y, and T_z can be identified. From the five surface oscillation frequencies and the three translational frequencies, the surface tension, σ, is determined by use of the formula by Cummings and Blackburn [7]:

$$\sigma = \frac{3M}{160\pi} \sum_{m=-2}^{2} \omega_i^2 - 1.9\Omega^2 - 0.3 \left(\frac{g}{R_0}\right)^2 \Omega^{-2}, \tag{3}$$

$$\text{with } \Omega^2 = \frac{1}{3}\left(T_x^2 + T_y^2 + T_z^2\right). \tag{4}$$

Here, g is the gravitational acceleration and R_0 is the sample radius. The different frequencies, ω_i, can be identified by employing selection rules. They are based on geometrical considerations and make use of the Fourier transforms of the sum and difference of two perpendicular radii [8]. A typical spectrum, displaying all these frequencies, is shown in Fig. 2.

Figure 3 shows the measured surface tensions of $Al_{46}Ti_{46}Nb_8$, $Al_{46}Ti_{46}Ta_8$, and $Ti_{90}Al_6V_4$ as functions of temperature.

In the temperature range considered, their temperature dependence is well described by a linear fit:

$$\sigma = \sigma_L + \sigma_T\,(T - T_L). \tag{5}$$

Numerical values for the fit parameters are given in Table 2. The results for $Ti_{90}Al_6V_4$ agree reasonably well with our previous measurements [9].

2.2.2 *Surface-Tension Measurements by the Combined Pendant/Sessile-Drop Method*

Due to the high value of melting temperatures and the presence of highly reactive elements, such as Ti, it is extremely difficult to perform measurements of surface tension of the AlTi-based alloys by applying conventional methods, such as the sessile- or the large-drop methods [10]. Using a modified sessile-drop (SD) technique, where the drop is released by a capillary dispenser onto an inert substrate, it was possible to overcome these problems and to measure surface tension by the PD and SD methods simultaneously.

In the present setup, a new, high-temperature furnace, employing a tantalum heater, was used, and the droplet was released from above by a capillary dispenser. In this configuration, the PD measurements were made. Then, the droplet was put in contact with the substrate by moving the capillary down and the substrate up. Next the droplet has been extended and broken by moving the capillary and the substrate in reverse directions. This is shown in Fig. 4. After drop deposition, the support was slightly rotated in order to better position the drop image as well as to check the drop symmetry, and the SD experiment was performed.

This methodology was never applied before to measure the surface tension of metals with high melting points, except for the measurements on a set of refractory elements [11]. However, the procedures of the drop formation and release, applied in this work,

Table 2 Surface-tension data of $Al_{46}Ti_{46}Nb_8$, $Al_{46}Ti_{46}Ta_8$, and $Al_6Ti_{90}V_4$ obtained by the sessile-drop, pendant-drop, and oscillating-drop methods, including results obtained under microgravity

Method	$Al_{46}Ti_{46}Nb_8$ ($T_L = 1{,}843$ K)		$Al_{46}Ti_{46}Ta_8$ ($T_L = 1{,}890$ K)		$Al_6Ti_{90}V_4$ ($T_L = 1{,}933$ K)	
	σ_L (N · m^{-1})	$-\sigma_T$ (10^{-4} N · m^{-1} · K^{-1})	σ_L (N · m^{-1})	$-\sigma_T$ (10^{-4} N · m^{-1} · K^{-1})	σ_L (N · m^{-1})	$-\sigma_T$ (10^{-4} N · m^{-1} · K^{-1})
Pendant drop	1.11 @ 2,007 K	–	1.15 @ 2,063 K	–	–	–
Sessile drop	1.07 @ 2,007 K	–	1.11 @ 2,089 K	–	–	–
Oscillating drop	1.11 @T_L	2.2	1.19 @T_L	1.9	1.33 @ T_L	3.6
Oscillating drop (μg)	1.16 @T_L	4.2	1.12 @T_L	4.0	1.49 @T_L	4.1

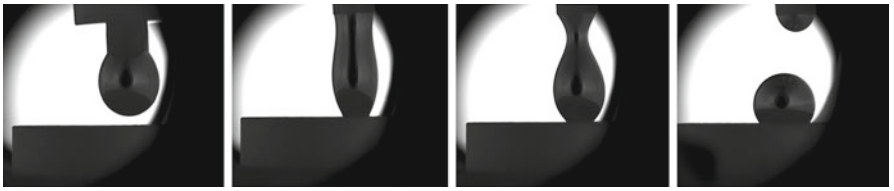

Fig. 4 Release of a pendant drop from the dispenser to the substrate

as well as the procedure for the determination of the surface-tension values based on the acquisition and analysis of the PD profile, differ substantially from the procedures and the analysis described in [11].

Surface-tension measurement by the PD combined method, as described above, has been performed under an atmosphere of flowing ArN60 for $Al_{46}Ti_{46}Nb_8$ and $Al_{46}Ti_{46}Ta_8$. In order to obtain freshly formed drops for surface-tension measurements under oxide-free conditions, the alloys have been squeezed from an alumina capillary immediately after alloy melting. They were overheated to 2,007 K, in order to squeeze the drops through the small hole of the capillary. At this temperature, the PD measurements were made. Subsequently, the droplets have been deposited on an Y_2O_3 treated alumina substrate by the procedure described above. The SD experiments have been carried out at $T = 2{,}063$ K for $Al_{46}Ti_{46}Nb_8$ and $T = 2{,}089$ K in the case of the $Al_{46}Ti_{46}Ta_8$ alloy. A variation of temperature in order to obtain the temperature coefficient σ_T was not possible, due to experimental difficulties.

The analysis of the images acquired each 0.1 s during the surface-tension measurements was used to obtain the surface-tension data by both the PD and the SD methods. Table 2 shows the values of the surface tension of $Al_{46}Ti_{46}Nb_8$ and $Al_{46}Ti_{46}Ta_8$ measured by both methods.

2.2.3 Discussion

As is evident from Table 2, excellent agreement exists between the different methods regarding the surface tension, σ. The scatter of the data is less than 4 %. On the other hand, there is a distinct difference between the temperature coefficient, σ_T, measured on ground and in microgravity. The reason for this effect is unclear. It may be either due to the fact that the Cummings correction, Eq. 3 does not have the correct temperature dependence, or that the transient measurement method employed during parabolic flights introduces undesired temperature gradients. It must also be stressed that the oxygen partial pressures in the two furnaces, used on ground and on-board the airplane, may be different. As is well known, the effect of oxygen partial pressure is more pronounced for the temperature coefficient than for the surface tension itself. Unfortunately, the SD and PD experiments cannot contribute to the clarification of this question, due to their own experimental difficulties. The ultimate answer will be given by systematic investigations of the oscillating-drop technique in microgravity on board the International Space Station.

3 Thermodynamic Modeling

3.1 Theoretical Background

Recently, geometric models, such as those of Kohler [12], Toop [13], and Chou [14], originally developed to predict the thermodynamic properties of ternary systems, have been also applied to calculate their thermophysical properties, such as the surface tension and viscosity. As concerns the surface properties, the surface tension of ternary alloys predicted by geometric models can be subsequently compared with the corresponding results calculated by using the models based on Butler's concept [15].

3.1.1 Geometric Models

The excess surface tension, ${}^{\mathrm{xs}}\sigma$, of melts is defined as the difference between the true surface tension and the corresponding value of the ideal solution. The excess surface tension of ternary alloy systems using Kohler's model is given by

$$ {}^{\mathrm{xs}}\sigma = \sum_{i=1}^{2} \sum_{j=i+1}^{3} (X_i + X_j)^2 ({}^{\mathrm{xs}}\sigma_{ij})_{X_i/X_j}, \tag{6} $$

where ${}^{\mathrm{xs}}\sigma_{ij}$ denotes the excess surface tension of the binary system $i - j$ for the ratio $X_i/X_j = x_i/x_j$. X_i and x_i represent the molar fraction i in the ternary and binary systems, respectively.

The binary contributions are described by polynomials as

$$ {}^{\mathrm{xs}}\sigma_{ij} = P_n(x_i = X_i/(X_i + X_j)), \tag{7} $$

where P_n is a Redlich–Kister polynomial given by

$$ P_n = x_i x_j \sum_{\nu=0}^{n} A_i (x_i - x_j)^{\nu}. \tag{8} $$

However, sometimes there may be a physical reason to divide the component elements into different groups. For example, if components 2 and 3 are similar to each other but differ markedly from component 1, then one should expect the binary systems 1–2 and 1–3 to be similar and it may be advantageous to describe the ternary 1–2–3 system in such a way that the expression would reduce to the binary expression if one could make 2 and 3 identical. Such a numerical method was proposed by Toop [13], and it is given by

$$ \begin{aligned} {}^{\mathrm{xs}}\sigma = {} & \frac{X_2}{1 - X_1} \cdot {}^{\mathrm{xs}}\sigma_{12}(X_1; 1 - X_1) + \frac{X_3}{1 - X_1} \cdot {}^{\mathrm{xs}}\sigma_{13}(X_1; 1 - X_1) \\ & + (X_2 + X_3)^2 \cdot {}^{\mathrm{xs}}\sigma_{23}\left(\frac{X_2}{X_2 + X_3}; \frac{X_3}{X_2 + X_3}\right). \end{aligned} \tag{9} $$

Chou proposed a general solution model to predict the thermodynamic properties of a ternary alloy system [14]. Chou's model introduces the concept of similarity coefficients, and a linear relation between selected binary compositions and the composition of ternary system. In this way, the problem of "asymmetry" or "non-symmetry" in a ternary system can be overcome. A reasonable assumption should be that the selected binary compositions are closely related to the ternary itself.

The excess surface tension is given by Chou's model as

$$^{xs}\sigma = \frac{X_1X_2}{X_{1(12)}X_{2(12)}} \cdot {}^{xs}\sigma_{12} + \frac{X_2X_3}{X_{2(23)}X_{3(23)}} \cdot {}^{xs}\sigma_{23} + \frac{X_3X_1}{X_{3(31)}X_{1(31)}} \cdot {}^{xs}\sigma_{31}, \quad (10)$$

where $X_i$is the mole fraction of component i in the ternary system, and $X_{i(ij)}$is the mole fraction of component i in the $i-j$ binary system, which can be calculated from the following equations,

$$\begin{aligned} X_{1(12)} &= X_1 + \frac{\eta_1}{\eta_1+\eta_2}X_3, \\ X_{2(23)} &= X_2 + \frac{\eta_2}{\eta_2+\eta_3}X_1, \\ X_{3(31)} &= X_3 + \frac{\eta_3}{\eta_3+\eta_1}X_2. \end{aligned} \quad (11)$$

The parameters η_i in Eq. 11 take into account the correlation with other components (j and k) of the ternary system,

$$\begin{aligned} \eta_1 &= \int_0^1 ({}^{xs}\sigma_{12} - {}^{xs}\sigma_{13})^2 \mathrm{d}X_1, \\ \eta_2 &= \int_0^1 ({}^{xs}\sigma_{21} - {}^{xs}\sigma_{23})^2 \mathrm{d}X_2, \\ \eta_3 &= \int_0^1 ({}^{xs}\sigma_{31} - {}^{xs}\sigma_{32})^2 \mathrm{d}X_3. \end{aligned} \quad (12)$$

3.1.2 Butler's Equation

Butler's equation has been extensively used to calculate the surface tension of binary and multicomponent alloy systems [15]. In this model, the surface is considered as an additional thermodynamic phase, in equilibrium with the bulk. All thermodynamic models, such as the regular solution model, the subregular solution model, the compound formation model, the self-aggregating model, etc. can be used in conjunction with Butler's equation [16–21].

Table 3 Thermodynamic data of the excess Gibbs energies (Redlich–Kister coefficients) on the Al–Ti–X (X = Nb, Ta, V) liquid phases

System	ν	${}^{\mathrm{xs}}G_{\mathrm{L}}^{\mathrm{A-B}}(\mathrm{J\cdot mol^{-1}})$	Reference
Ti–Al	0	$-118048 + 41.972T$	[23]
	1	$-23613 + 19.704T$	
	2	$34757 - 13.844T$	
Al–Nb	0	$-91000 + 25T$	[22]
	1	6000	
	2	15000	
Nb–Ti	0	$8500 + 30T$	[22]
Al–Ta	0	-108000	[22]
	1	6000	
	2	17000	
Ta–Ti	0	1000	[22]
	1	-7000	
Al–V	0	$-50725 + 9T$	[22]
	1	$-15000 + 8T$	
Ti–V	0	1400	[22]
	1	-4100	

Table 4 Surface-tension reference data of pure metals

Surface tension				
Pure metal	Melting point (K)	σ_{L} $(\mathrm{N\cdot m^{-1}})$	$-\sigma_T$ $(\mathrm{N\cdot m^{-1}\cdot K^{-1}})$	Reference
Al	933	0.867	0.15×10^{-3}	[25]
Ti	1,943	1.557	0.156×10^{-3}	[26]
Nb	2,742	1.900	0.199×10^{-3}	[26]
Ta	3,288	2.010	0.23×10^{-3}	[27]
V	2,175	1.900	0.25×10^{-3}	[27]

Based on Butler's model, the surface tension of liquid alloys can be calculated by

$$\sigma = \sigma_i + \frac{RT}{S_i} \ln \frac{X_i^{\mathrm{s}}}{X_i^{\mathrm{b}}} + \frac{1}{S_i}[G_i^{\mathrm{xs,s}}(T, X^{\mathrm{s}}_{j(j=2,3)}) - G_i^{\mathrm{xs,b}}(T, X^{\mathrm{b}}_{j(j=2,3)})], \quad i = 1, 2, 3 \tag{13}$$

where R, T, σ_i, and S_i are the universal gas constant, temperature, surface tension of pure component i, and surface area of component i, respectively. The surface area of component i is calculated from Avogadro's number N_0, the atomic mass, and density data, as

$$S_i = 1.091 N_0 \left(\frac{M_i}{\rho_i}\right)^{2/3}. \tag{14}$$

Table 5 Calculated surface tensions (in $N \cdot m^{-1}$) of liquid Al–Ti–X alloys at $T = 2{,}073$ K together with the surface-tension experimental data

Kohler model	Toop model	Chou model	Butler model	Oscillating drop	Sessile drop	Pendant drop
$Al_{46}Ti_{46}Nb_8$						
1.05 $T = 2{,}073$ K	0.99 $T = 2{,}073$ K	1.04 $T = 2{,}073$ K	1.02 $T = 2{,}073$ K	1.11 $T = 1{,}843$ K	1.12 $T = 2{,}007$ K	1.11 $T = 2{,}007$ K
$Al_{46}Ti_{46}Ta_8$						
1.14 $T = 2{,}073$ K	1.02 $T = 2{,}073$ K	1.08 $T = 2{,}073$ K	1.04 $T = 2{,}073$ K	1.19 $T = 1{,}890$ K	1.15 $T = 2{,}089$ K	1.11 $T = 2{,}063$ K
$Al_6Ti_{90}V_4$						
1.51 $T = 2{,}073$ K	1.36 $T = 2{,}073$ K	1.41 $T = 2{,}073$ K	1.38 $T = 2{,}073$ K	1.33 $T = 1{,}933$ K		

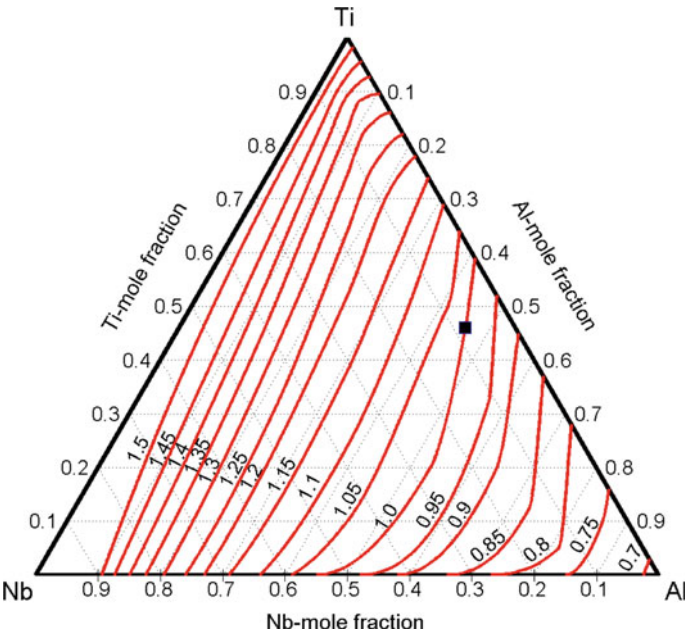

Fig. 5 Iso-surface tension lines of liquid Al–Ti–Nb alloys calculated by Butler's equation for the regular solution model at 2,073 K. The *square symbol* represents the composition location of the $Al_{46}Ti_{46}Nb_8$ (at%) in the Gibbs triangle and the corresponding surface tension calculated value

$G_i^{\mathrm{xs,s}}(T, X^{\mathrm{s}}_{j(j=2,3)})$ and $G_i^{\mathrm{xs,b}}(T, X^{\mathrm{b}}_{j(j=2,3)})$ are partial excess Gibbs energies of i in the surface phase as a function of T and $X^{\mathrm{s}}_{j(j=2,3)}$ and that of i in the bulk phase as a function of T and $X^{\mathrm{b}}_{j(j=2,3)}$. The excess energy term of a component i can be derived from the standard thermodynamic relation, in the form,

$$G_i^{\mathrm{xs}} = G^{\mathrm{xs}} + \sum_{j=1}^{n} (\delta_{ij} - X_j) \frac{\partial G^{\mathrm{xs}}}{\partial X_j}, \tag{15}$$

where $\delta_{ij}$is Kronecker's symbol.

The surface partial Gibbs energy is approximated by

$$G_i^{\mathrm{xs,s}} = \beta G_i^{\mathrm{xs,b}}. \tag{16}$$

β is a parameter taking into account the reduced coordination at the surface. According to Tanaka [19], we take $\beta = 0.75$.

Thermodynamic data on the Gibbs excess free energies of the Al–Ti–X (X = Nb, Ta, V) binary subsystems are given in the form of Redlich–Kister polynomials, in the form,

$$^{\mathrm{xs}}G_{\mathrm{L}}^{\mathrm{A-B}} = x_i x_j \sum_{\upsilon=0}^{n} (A_\upsilon + B_\upsilon T)(x_i - x_j)^\upsilon. \tag{17}$$

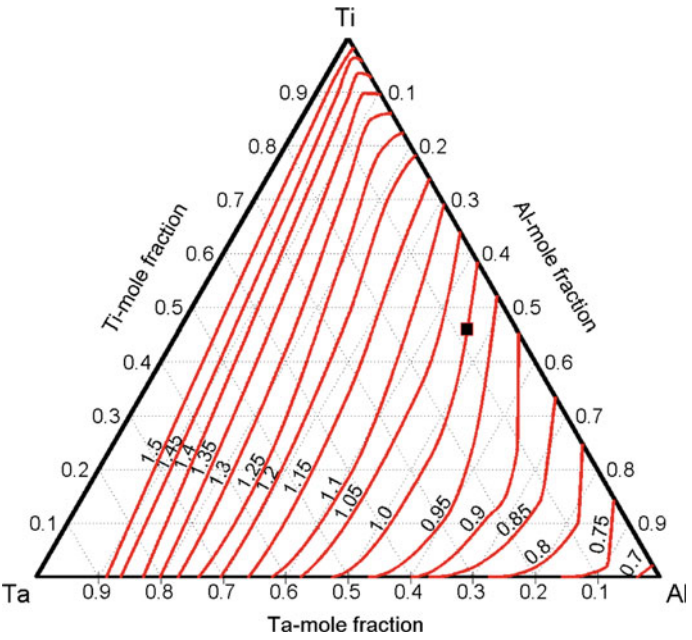

Fig. 6 Iso-surface tension lines of liquid Al–Ti–Ta alloys calculated by Butler's equation for the regular solution model at 2,073 K. The *square symbol* represents the composition location of the $Al_{46}Ti_{46}Ta_8$ (at%) in the Gibbs triangle and the corresponding surface tension calculated value

Due to the lack of experimental data, the Gibbs excess free energies of the ternary systems were calculated combining the corresponding binary values, without any additional ternary contribution;

$$^{xs}G_{L}^{A-B-C} = \sum_{i,j} x_i x_j \sum_{\upsilon=0}^{n} (A_\upsilon + B_\upsilon T)(x_i - x_j)^\upsilon. \tag{18}$$

3.2 Surface Tension of Liquid Al–Ti–X Ternary Alloys

In order to predict the surface tension of liquid Al–Ti–X ternary alloys, all aforementioned models (Kohler, Toop, Chou, and Butler) have been applied. Except for Al–Ti, the excess Gibbs energy terms of the liquid binary phases were taken from [22], while the liquid phase of Al–Ti was described by [23]. The data on the melting temperatures, densities, and molar volumes were taken from [24], while the surface-tension reference data of liquid Al [25], Ti, Nb [26], and Ta, V [27] were obtained by different experimental methods; accordingly, it was not possible to estimate correctly an overall error of the calculated surface-tension values.

The input data used for the calculations of the surface tension of the ternaries and the corresponding binary subsystems are reported in Tables 3 and 4.

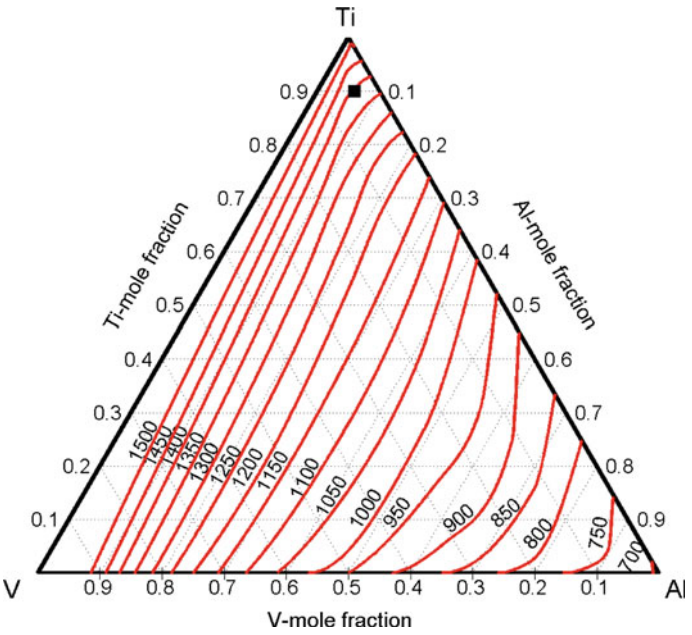

Fig. 7 Iso-surface tension lines of liquid Al–Ti–V alloys calculated by Butler's equation for the regular solution model at 2,073 K. The square symbol represents the composition location of the $Al_6Ti_{90}V_4$ (mass %) in the Gibbs triangle and the corresponding surface tension calculated value

The surface tensions of liquid Al–Ti–Nb, Al–Ti–Ta, and Al–Ti–V alloys have been calculated at $T = 2{,}073$ K by the Kohler, Toop, Chou, and Butler models in the regular solution approximation combining the corresponding data of the binary subsystems. It is important to mention that according to the equilibrium phase diagrams, some binary compositions correspond to solid phases. In such cases, of course, the calculations refer to an undercooled liquid phase. The results of calculations related to the ternary Al–Ti–Nb system are given in Table 5.

The surface-tension experimental data of liquid $Al_{46}Ti_{46}Nb_8$ have been measured by EML over an extended temperature range, while those obtained by SD and PD methods are from the measurements performed at only one temperature. The experimental surface-tension data are close to each other. Comparing the predicted surface-tension values with the corresponding experimental data, the best agreement is found for the Kohler model.

Generally speaking, the estimated values tend to be lower than the measured values for the alloys. On the one hand, this may be due to the fact that the values quoted in Table 4 for the pure elements are too low. Some authors cite a much higher value for pure Al than that given in Table 4, and Paradis [28] quotes a higher value for Ta. On the other hand, Al is known to reduce the solubility of oxygen in binary alloys significantly; thus, the dissolved oxygen levels in the alloys may be significantly lower than those in the component metals. This would lead to an increase in the surface tension of the alloy and may account for the difference between the estimated and measured values.

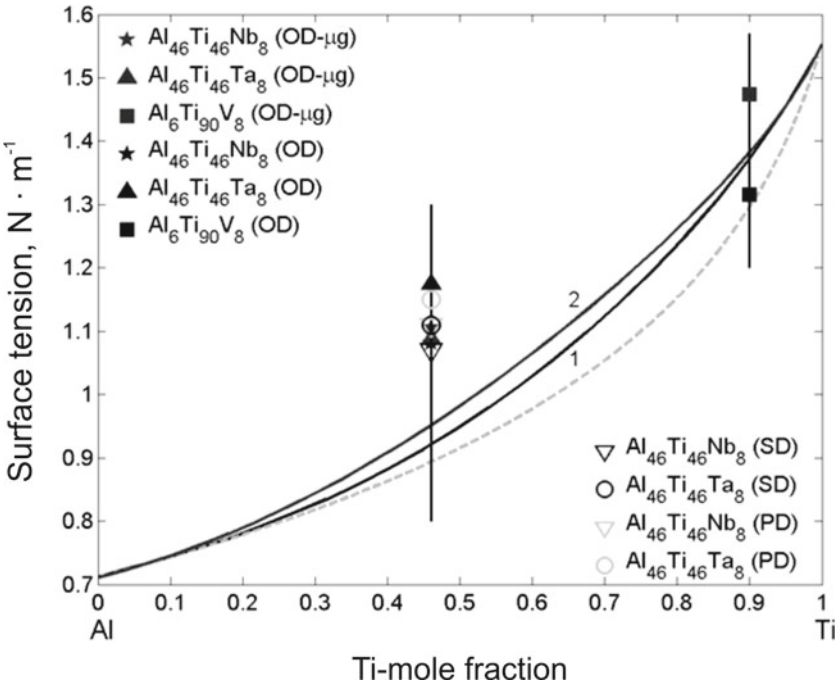

Fig. 8 Experimental surface tension values of liquid $Al_{46}Ti_{46}Nb_8$, $Al_{46}Ti_{46}Ta_8$, and $Al_6Ti_{90}V_4$ alloys obtained by different experimental techniques (OD, OD-μg, SD, and PD). For a comparison are shown the Al–Ti isotherms (1-regular solution; 2-compound formation model; ------ ideal solution model) calculated at 1,973 K

In order to analyze the surface-tension variations with composition, iso-surface tension lines of the alloys have been calculated by the regular solution model at $T = 2{,}073$ K (Fig. 5). The experimental data of the surface tension of the $Al_{46}Ti_{46}Nb_8$ alloy, measured by DLR using the EML technique, differs about 6 % from the corresponding predicted values. As can be expected, the experimental data obtained at lower temperatures by the SD and PD techniques, exhibit slightly larger differences with respect to the predicted values.

The experimental data of the surface tension of the $Al_{46}Ti_{46}Ta_8$ alloy, measured by DLR using the EML technique differs about 14 % from the corresponding predicted values (Fig. 6). The bigger difference between the experimental and theoretical surface-tension values, observed in the case of the $Al_{46}Ti_{46}Ta_8$ alloy can be attributed to a large uncertainty of Ta surface-tension data with respect to that of Nb, taken as the reference data in the present calculations.

Finally, the iso-surface tension lines for the system $Ti_{90}Al_6V_4$ are shown in Fig. 7.

In order to establish the effects of the third component (Nb, Ta, and V) on the experimental surface tension values of the ternary alloys, the experimental data obtained by different methods have been compared with corresponding binary AlTi alloys with the same Ti content. The presence of Nb and Ta significantly increases the

surface tension of ternary alloys (Fig. 8). It is well known that the presence of short-range-order phenomena in the liquid phase may increase the surface tension of melts. Although the structural experimental data on these ternary alloys are lacking, the presence of the short-range-order phenomena in their binary subsystems may indicate similar effects of these phenomena on the surface tension of AlTiNb and AlTiTa alloys.

4 Summary

The surface tension and density of three representative AlTi-based alloys were measured in the liquid phase, using EML and an advanced high-temperature furnace. Results obtained by both methods show excellent agreement. The binary Al–Ti system has been modeled thermodynamically, and predictions for the surface tension as a function of composition were made. By comparing with the experimental data, the influence of the addition of a third, refractory, element becomes evident.

Acknowledgments Part of this work was carried out under contract FP6-500635-2 of the European Commission within the IMPRESS project. The authors are grateful to one of the referees for pointing out the possible reasons for the discrepancy between estimated and measured surface tension values.

References

1. Ti-2007 Science and Technology, Proceedings of the 11th World Conference on Titanium, Kyoto, Japan, 2007, ed. by M. Niinomi, S. Akiyama, M. Hagiwara, M. Ikeda, K. Maruyama (The Japan Institute of Metals, Sendai, 2007)
2. M. Long, H.J. Rack, Biomaterials **19**, 1621 (1998)
3. D. Jarvis, Mater. World 11 (2005)
4. J. Brillo, I. Egry, Int. J. Thermophys. **24**, 1155 (2003)
5. R. Harding, R. Brooks, G. Pottlacher, J. Brillo, in *Gamma Titanium Aluminides*, ed. by Y. Kim, H. Clemens, A. Rosenberger (TMS, Warrendale, PA, 2003), p. 75
6. D.M. Herlach, R.F. Cochrane, I. Egry, H.J. Fecht, A.L. Greer, Int. Mater. Rev. **38**, 273 (1993)
7. D.L. Cummings, D.A. Blackburn, J. Fluid Mech. **224**, 395 (1991)
8. S. Sauerland, K. Eckler, I. Egry, J. Mater. Sci. **11**, 330 (1992)
9. S. Schneider, I. Egry, I. Seyhan, Int. J. Thermophys. **23**, 1241 (2002)
10. Yu.V. Naidich, Prog. Surf. Membr. Sci. **14**, 353 (1981)
11. J.P. Garandet, B. Vinet, P. Gros, J. Colloid Interf. Sci. **165**, 351 (1994)
12. F. Kohler, Monatsch. Chem. **91**, 738 (1960)
13. G.W. Toop, Trans. AIME **233**, 450 (1965)
14. K.-C. Chou, Calphad **19**, 313 (1995)
15. J.A.V. Butler, Proc. R. Soc. A **135**, 348 (1932)
16. R.N. Singh, Can. J. Phys. **65**, 309 (1987)
17. R.N. Singh, F. Sommer, Rep. Prog. Phys. **60**, 57 (1997)
18. R. Speiser, D.R. Poirier, K. Yeum, Scr. Metall. **21**, 687 (1987)
19. T. Tanaka, K. Hack, S. Hara, MRS Bull. April, 45 (1999)
20. I. Egry, J. Brillo, T. Matsushita, Mater. Sci. Eng. A **413–414**, 460 (2005)
21. R. Novakovic, E. Ricci, D. Giuranno, A. Passerone, Surf. Sci. **576**, 175 (2005)
22. N. Saunders COST 507, *Thermochemical Database for Light Metal Alloys*, ed. by I. Ansara, A.T. Dinsdale, M.H. Rand, vol. 2 (European Union, Luxembourg, 1998)
23. V.T. Witusiewicz, A.A. Bondar, U. Hecht, S. Rex, T. Ya Velikanova, J. Alloys Compd. **465**, 64 (2008)
24. T. Iida, R.I.L. Guthrie, *The Physical Properties of Liquid Metals* (Clarendon Press, Oxford, 1993)
25. G. Lang, P. Laty, J.C. Joud, P. Desré, Z. Metall. **68**, 113 (1977)

26. T. Ishikawa, P.-F. Paradis, T. Itami, S. Yoda, J. Chem. Phys. **118**, 7912 (2003)
27. B. Vinet, L. Magnusson, H. Fredriksson, P.J. Desré, J. Colloid Interf. Sci. **255**, 363 (2002)
28. P.-F. Paradis, T. Ishikawa, S. Yoda, J. Appl. Phys. **97**, 053506 (2005)